Calculation of exchange integrals and electronic structure for manganese ferrite

Xu Zuo and Carmine Vittoria
Department of Electrical and Computer Engineering, Northeastern University, Boston, Massachusetts 02115
(Received 7 June 2002; revised manuscript received 12 September 2002; published 18 November 2002)

The electrical and magnetic properties of manganese ferrite ($MnFe_2O_4$) are calculated with the density-functional theory (DFT) method for both normal and inverse spinel structures. The exchange functional is chosen to be a mixture of Becke exchange and Fock exchange with variable weight (w). The exchange integrals J_{AB} (the exchange integral between the nearest-neighbor A and B sites) and J_{BB} (the exchange integral between nearest-neighbor B sites) are calculated by substituting the total energies of different magnetic ground states into the Heisenberg model. The calculated value of J_{AB} is in agreement with the experimental values measured by neutron diffraction and NMR. Also, the parameters U (Coulomb repulsion energy), Δ (charge-transfer energy), and E_G (band gap) are extracted from the density of states (DOS) and plotted versus w. Our calculated band gap shows that $MnFe_2O_4$ is a complex insulator, in contrast to previous local spin-density approximation and generalized gradient approximation calculations, which showed it to be half metallic.

DOI: 10.1103/PhysRevB.66.184420 PACS number(s): 75.30.Et, 75.50.Gg, 71.20.Ps, 71.15.Mb

I. INTRODUCTION

Manganese ferrite is a well-known microwave ferrite material with a spinel crystallographic structure (space group $Fd3m$), in which O^{2-} form tetragonal and octagonal local symmetries that are referred to as A and B sites, respectively.[1] A normal spinel structure, per primary cell, consists of two A sites occupied by two Mn^{2+} and four B sites each occupied by four Fe^{3+}. On the other hand, an inverse spinel structure, per primary cell, consists of two A sites occupied by two Fe^{3+} and four B sites occupied by both two Mn^{2+} and two Fe^{3+} ions. Experiments have shown that manganese ferrite bulk material existed in a mixture of normal and inverse spinel structures and that the range of inverse spinel structure varied around 20%, depending on the details of material preparation.[2] Although this ferrite material has had a niche in microwave technology for a long time,[3,4] the basic mechanisms behind the ferrimagnetic and insulating ground states have only been understood in the frame of the Hubbard model.[5–7] The superexchange interaction[5,8–10] between A and B sites as implied in the Hubbard model gives rise to an antiferromagnetic J_{AB}, which is much stronger than antiferromagnetic J_{BB} and J_{AA} due to the local symmetries of A and B sites and the crystal structure. Consequently, it yielded a ferrimagnetic ground state[1] as observed in neutron-diffraction experiments.[2] At the same time, the on-site Coulomb repulsion in the Hubbard model splits the half filled d bands of Fe^{3+} and Mn^{2+} into full and empty subbands with opposite spins, and thus, gives rise to a band gap at the Fermi level, referred to as a Mott insulator.[11–15] The insulating property of this material has been confirmed by activation energy experiments.[16] Also, since Mn and Fe belong to later $3d$ transition metals, $MnFe_2O_4$ may be classified as a charge-transfer insulator[17–21] in which the d-d transfers between magnetic ions are via the intervening ligand through p-d hybridization.[22–25] Regardless of whether $MnFe_2O_4$ is a Mott or charge-transfer insulator, a reliable quantitative calculation of exchange integrals and energy gaps requires an accurate estimation of the transfer integral (t), on-site Coulomb repulsion (U), and charge-transfer energy (Δ), which may not be available in the framework of the Hubbard model self-consistently.

Band calculations have been rather successful in quantitatively estimating the electronic structure of nonmagnetic materials, if the electron-electron interaction was properly approximated by a single-electron Hamiltonian. However, in practical calculations for transition-metal oxides, the results are rarely in agreement with experiments due to the single-electron approximation, and sensitive to forms of exchange and correlation functionals. For example, Hartree-Fock[26–29] (HF) calculations usually yield an antiferromagnetic exchange integral weaker than the experimental value, and give rise to a larger band gap. For nickel monoxide (NiO), HF yielded a J_2 (exchange integral between next-nearest neighbors) of 49 K,[30] compared to 221 K given by magnon dispersion measurement,[31] a band gap of about 14 eV,[30] compared to about 4.0 eV as measured by an optical reflectance spectrum,[32] or photoemission spectroscopy (PES) and bremsstrahlung isochromat spectroscopy (BIS).[18,33] On the other hand, local spin-density approximation[34–37] (LSDA) usually gives rise to a band gap smaller than experimental values. When the LSDA is applied to NiO, the band gap is about 0.9 eV;[38–40] much smaller than the experimental value. Several corrections to the LSDA, such as the self-interaction correction (SIC),[41,42] generalized gradient approximation[43–48] (GGA), and LSDA+U (Ref. 49) were intended to improve the band gap. However, in LSDA+U,[49–52] U is an *ad hoc* parameter. The SIC and GGA are not sufficient to open the energy gap as large as the experimental value. For NiO, the band gap is 2.54 by SIC (Refs. 53 and 54) and 1.2 eV by GGA.[55]

Moreover, the shortcoming in which most of the above calculations failed to predict the correct band-gap and exchange integrals for later $3d$ transition metal oxides can be traced to the inaccurate predictions of predicting U and t. HF overestimates U and LSDA underestimates U. For NiO, HF yields $U \sim 27.9$ eV (Ref. 30) and LSDA yields $U \sim 2$ eV,[38–40] compared to 7–9 eV measured from PES and BIS experiments.[18,33] HF underestimates t and LSDA overestimates t. For NiO, since the contribution to t is substan-

tially the covalence effect between Ni^{2+} and O^{2-} and the covalence effect of t_{2g} orbits is negligible, t is proportional to the crystal-field split (Δ_{CF}) approximately.[5] HF yields $\Delta_{CF} \sim 0.012$ hartree ≈ 0.33 eV[30] and LSDA yields $\Delta_{CF} \sim 1.3$ eV,[40] compared to $8500\ cm^{-1} \approx 1$ eV for $[Ni(H_2O)_6]^{2+}$ (Ref. 56) or $7250\ cm^{-1} \approx 0.9$ eV for $KNiF_3$.[57] Since HF underestimates t and overestimates U, according to the Hubbard model it underestimates the superexchange interaction and overestimates the band gap. On the other hand, since LSDA overestimates t and underestimates U, according to the Hubbard model it overestimates superexchange interaction and underestimates band gap.

In fact, in a solid, U can be obtained by renormalizing the on-site Coulomb repulsion of the bare ions (U_b) in a noninteracting system, which is given by

$$U = \frac{U_b}{1 + U_b/G}, \tag{1}$$

where G is the Green function that takes the electron-electron interaction into account.[7] In HF, since the electron-electron correlation is neglected, U is equal to U_b, which is equivalent to $G \rightarrow \infty$. When the electron-electron correlation is increasing, G is finite but decreasing in value. For transition metals, Kanamori estimated $U \sim W$, where W is the bandwidth of the d band, which is much smaller than U_b.[7] In LSDA, the overemphasized electron-electron correlation yields $G \sim W$, which is much smaller than U_b, and, consequently, yields $U \sim W$.[40] Also, Δ_{CF} can be interpreted as the different p-d hybridization strength for the e_g and t_{2g} orbits.[17] Thus, any underestimation or overestimation of hybridization may yield an incorrect Δ_{CF}. From the result of Δ_{CF}, it is obvious that the hybridization is underestimated in HF but overestimated in LSDA. This is consistent with the underbinding problem of HF (Refs. 30 and 58) or the overbinding problem of LSDA,[59,60] which is also due to the underestimation in HF or overestimation in LSDA for the electron-electron correlation. Thus, the failures of the above calculations in later $3d$ transition-metal oxides are inherited by the exchange-correlation functional chosen to approximate the electron-electron interaction. From the results of the band gap, SIC and GGA are more accurate than both LSDA and HF in approximating the electron-electron correlation, but still insufficient for transition-metal oxides. However, a mixture of Fock exchange and LSDA may be the proper approximation in insulating transition metal oxides, since it is based on the linear interpolation of the adiabatic relation of Kohn-Sham density-functional theory.[61,62] In this paper, our calculation is based on the mixture of Fock exchange and Becke exchange for $MnFe_2O_4$. We calculated J_{AB}, J_{BB}, E_G, U, and Δ as a function of w. We find that J_{AB} and J_{BB} agree with the experimental values, and that $MnFe_2O_4$ is an insulator.

II. APPROACH

We choose a modified version of Becke's parametrization of the exchange-correlation approximation, which is examined for a wide range of atoms and molecules.[62] In this approximation, the correlation part is given by

$$E_C = E_C^{\mathrm{LSDA}} + 0.81 \Delta E_C^{\mathrm{PW}}, \tag{2}$$

where E_C^{LSDA} and ΔE_C^{PW} are LSDA correlation and Perdew-wang GGA (PWGGA) correction, respectively.[44,45] The exchange part is given by

$$E_X = (1-w)(E_X^{\mathrm{LSDA}} + 0.9 \Delta E_X^B) + w E_X^{\mathrm{exact}}, \tag{3}$$

where E_X^{exact}, E_X^{LSDA}, and ΔE_X^B are exact exchange, LSDA exchange, and Becke gradient correction,[47,48] respectively. In Becke's original parametrization, 0.81, 0.9, and $w = 0.2$ are determined from the least-squares fitting of atomization energies, ionization potentials, and proton affiliates.[62] In this paper, we are allowing w to vary between 0 and 1 to fit the experimental value of J_{AB} and J_{BB}. In the calculation, E_X^{exact} is replaced by the Fock exchange (E_x^F) according to the argument that the exact exchange, the exchange of the noninteracting Kohn-Sham reference system, is approximately equal to the Fock exchange.[59,60] We choose local Gaussian basis sets for Mn^{2+}, Fe^{3+}, and O^{2-}. The basis set of Mn^{2+} (86-411d41G) was optimized for MnO (Ref. 30) and $KMnF_3$. The basis set of Fe^{3+} (86-411d41G) was optimized for Fe_2O_3.[63] The basis set of O^{2-} (8-411G) was optimized for a wide range of oxide materials including MnO and NiO. The calculations were implemented by the CRYSTAL98 code[64] with experimental geometry,[65] where the lattice constant $a = 8.511$ Å and the position of O^{2-} is $u = 0.3846$, in a self-consistent spin-dependent scheme, in which the net spin in a primary cell is locked at the theoretical value of a simple ionic model. For example, if we designate the system to have an assumed ferromagnetic structure, the net spin in a primary cell will be locked at 30. In the calculation, we found that the convergence depends on the magnetic structure assigned to the lattice and w. For example, for the assumed ferromagnetic structure, any value of w yielded convergence. For the experimental ferrimagnetic structure, a value of w smaller than 40% caused divergence. The divergence was the result of the conflict between the highly localized basis sets (optimized by HF) and LSDA terms in the Hamiltonian that favor delocalized states. To improve the convergence and avoid time-consuming optimization for every w, we expanded the $3d$ part of the Fe^{3+} basis set up to 130% in the radial direction. This adjustment of basis set improves the value of J_{BB} toward the experimental value.

III. CALCULATED RESULTS

A. Magnetic properties

One of our main focuses in this calculation was to be able to explain numerically the observed values of J_{AB} and J_{BB} in $MnFe_2O_4$. We were only concerned with J_{AB} and J_{BB}, since there was no experimental data for J_{AA} with which to compare. To determine J_{AB} and J_{BB}, we calculated the ground-state energies of three different magnetic structures denoted as FM, FI-1, and FI-3. FM is the assumed ferromagnetic structure, in which all the spins in the A and B sites in a primary cell are parallel to each other. FI-1 is the observed ferrimagnetic structure in experiments, in which the spins

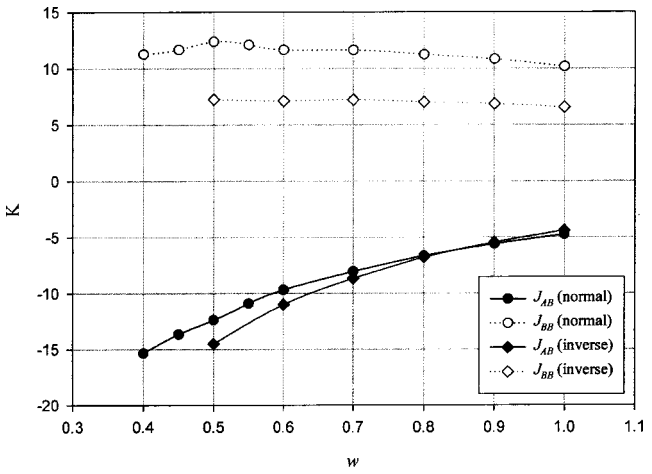

FIG. 1. J_{AB} and J_{BB} of normal and inverse structures using the basis set optimized by HF.

within A and B sublattices are aligned parallel, but are aligned antiparallel between them. FI-3 is an assumed ferrimagnetic structure, in which the spins within the A sublattice are aligned parallel and spins within the B sublattice are aligned antiparallel. Structure FI-2, where the spins within the A sublattice are aligned antiparallel, is not considered, since J_{AA} is not of interest here. Assuming the spin arrangement is collinear and substituting each magnetic structure into the Heisenberg model, we obtain

$$J_{AB}=\frac{1}{96S^2}(E_{\text{FI-1}}-E_{\text{FM}}),$$

$$J_{BB}=\frac{1}{32S^2}\left[E_{\text{FI-3}}-\frac{(E_{\text{FI-1}}+E_{\text{FM}})}{2}\right], \tag{4}$$

where $S=\frac{5}{2}$ is assumed according to the ionic model. The calculated J_{AB} and J_{BB} are plotted as a function of w in Fig. 1 for a normal spinel structure using optimized basis sets. The calculated J_{AB} is negative (antiferromagnetic) for all values of w, and becomes stronger when w decreases. In the case of pure Fock exchange ($w=100\%$), $J_{AB}=-4.7$ K is obtained. The calculation will diverge if w is smaller than 40% for FI-1 and FI-3 structures. At $w=40\%$, $J_{AB}=-15.3$ K is obtained, which is reasonable if compared to $J_{AB}=-22.7$ K obtained from nuclear magnetic resonance[66] and $J_{AB}=-19.1$ K as measured from magnon dispersion.[67,68] However, our calculated J_{BB} was always positive ($\sim$10 K), representing a ferromagnetic J_{BB}, which is not in agreement with the experimental value of -3.0 K.[66] In fact, when w decreases from 100%, J_{BB} first increases slightly and reaches a maximum at 50% and then decreases slightly. For inverse spinel structure, where we assumed all Mn^{2+} are on B sites (100% inverse), we obtained $J_{AB}=-4.4$ K at $w=100\%$ and $J_{AB}=-14.5$ K at $w=50\%$ (Fig. 1). When w was chosen to be smaller than 50%, the self-consistent iteration is divergent. As in the normal spinel structure, when w decreased, the antiferromagnetic J_{AB} becomes stronger, but J_{BB} was always positive ($\sim$7 K).

The above results are explained in terms of the competition between direct exchange and superexchange interactions between spins at A and B sites. As discussed in the introduction, HF underestimates t and overestimates U and consequently underestimates the superexchange contribution to J_{AB}. Since the distance between an A site and its nearest-neighbor B site is 3.5 Å and the bonding angle of A-O-B is 122.0°, the direct exchange contribution to the exchange integral is negligible. Thus, we obtain an antiferromagnetic J_{AB} even using only the Fock exchange, although the value of J_{AB} is about 20% of the experimental value. On the other hand, since the distance between the nearest-neighbor B sites is 3 Å and the bonding angle of B-O-B is 94.5°, the direct exchange exceeds the superexchange contribution underestimated by HF. Thus, a pure Fock exchange leads to a qualitatively incorrect ferromagnetic J_{BB}. This conclusion is applicable to manganese monoxide (MnO) also. In MnO, J_2 (the exchange integrals between the next-nearest-neighbor Mn^{2+} ions with a 180° Mn-O-Mn bond) given by HF is -1.4 K, compared to the experimental value of -4.8 K. On the other hand, J_1 (the exchange integrals between nearest-neighbor Mn^{2+} ions with a 90° Mn-O-Mn bond) given by HF is -0.19 K,[30,69] compared to the experimental value of -4.2 K.[70,71] However, when w decreases, the underestimation of superexchange is compensated by the LSDA contribution contained in the Becke exchange, since pure LSDA usually overestimates t and underestimates U and, consequently, overestimates the superexchange contribution to the exchange integrals. Therefore, in the case of J_{AB}, since the direct exchange is negligible, the antiferromagnetic J_{AB} becomes more and more negative or antiferromagnetic when w decreases. However, in the case of J_{BB}, the contributions from both direct exchange and superexchange increase and tend to cancel each other when w decreases. As a result, J_{BB} is always positive for both normal and inverse spinel structures.

J_{BB} for an inverse spinel structure is usually about 35%–40% smaller than that of the normal spinel structure at the same value of w. It is noted that the $3d$ wave functions of Fe^{3+} and Mn^{2+} are almost the same except that the $3d$ wave functions of Mn^{2+} are more extensive in the radial direction. The improvement of J_{BB} for the inverse spinel structure could be due to the expansion of $3d$ wave functions of magnetic ions at B sites. Thus, we expect that expanding the $3d$ wave function of Fe^{3+} in a radial direction will improve J_{BB} toward the experimentally observed antiferromagnetic value. We have expanded the $3d$ wave function of Fe^{3+} in the radial direction by a nonlinear regression fitting of scaled original wave functions. In detail, we define the expanded $3d$ wave function $\tilde{R}(r)$ as

$$\tilde{R}(r)=\lambda^{3/2}R(\lambda r), \tag{5}$$

where λ denotes the scaling factor and $R(r)$ is the original wave function. Both $R(r)$ and $\tilde{R}(r)$ are defined by a linear combination of four Gaussian-type orbit with four exponential and four contraction parameters. We found that expand-

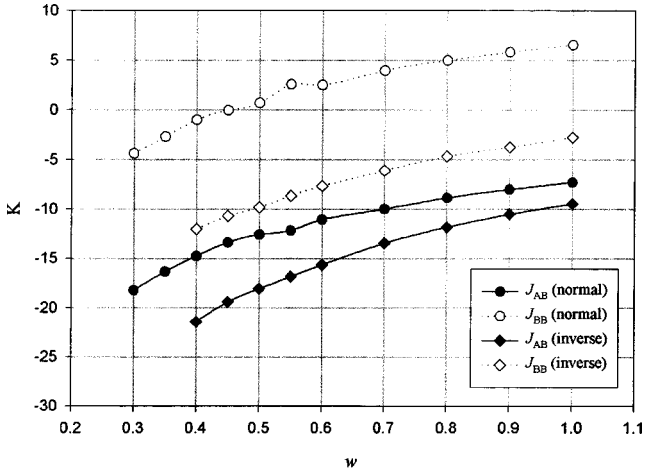

FIG. 2. J_{AB} and J_{BB} of normal and inverse structures using the basis set in which the $3d$ wave function of Fe^{3+} is expanded to 130% in the radial direction.

ing the $3d$ wave function of Fe^{3+} improved the calculated value of J_{BB} for both normal and inverse spinel structures. For the normal spinel structure, using $\lambda = 1/1.3$, we obtain $J_{AB} = -18.3$ and $J_{BB} = -4.4$ K at $w = 30\%$, which are quantitatively in agreement with experimental values (Fig. 2). For the inverse spinel structure, using $\lambda = 1/1.3$ we obtain $J_{AB} = -21.4$ K at $w = 40\%$, which is also qualitatively in agreement with experimental values (Fig. 2). We also note that the expanding $3d$ wave function improved the convergence of the calculation. For example, with $\lambda = 1/1.3$ the calculation is convergent at $w = 0.30$ for the normal spinel structure.

B. Electronic structure

So far we have shown that our calculation can lead to values of J_{AB} and J_{BB} in agreement with experiments. Without changing any parameters, we want to show that our calculation can also lead to values of E_G, U, and Δ consistent with experiments.

First, we consider the Mulliken population of a FI-1 magnetic structure calculated using optimized basis sets. Since the calculation was spin dependent, it is necessary to denote the Mulliken population of spin-up and -down electrons as n_α and n_β, respectively. The polarized $(n_\alpha - n_\beta)$ and depolarized $(n_\alpha + n_\beta)$ Mulliken populations of Mn^{2+} and Fe^{3+} versus w (Fig. 3) show that, when w decreases, the divergence between our calculation and the ionic model increases. This divergence is due to the hybridization between the d orbits of the magnetic ions and the orbits of the O^{2-} ions. For example, the calculated polarized Mulliken populations for either Mn^{2+} or Fe^{3+} given by our calculation are smaller than 5 (the value predicted by the ionic model), and decrease when w decreases. For $w = 40\%$, the polarized Mulliken population (net spin) of Fe^{3+} is 4.45 and -4.75 for Mn^{2+}, but for $w = 100\%$, the net spin of Fe^{3+} is 4.72 and -4.87 for Mn^{2+}. The calculated depolarized Mulliken populations of Mn^{2+} and Fe^{3+} are larger than 23 (including the core electrons), the value predicted by the ionic model, and increase when w decreases. Moreover, as predicted by crystal-field

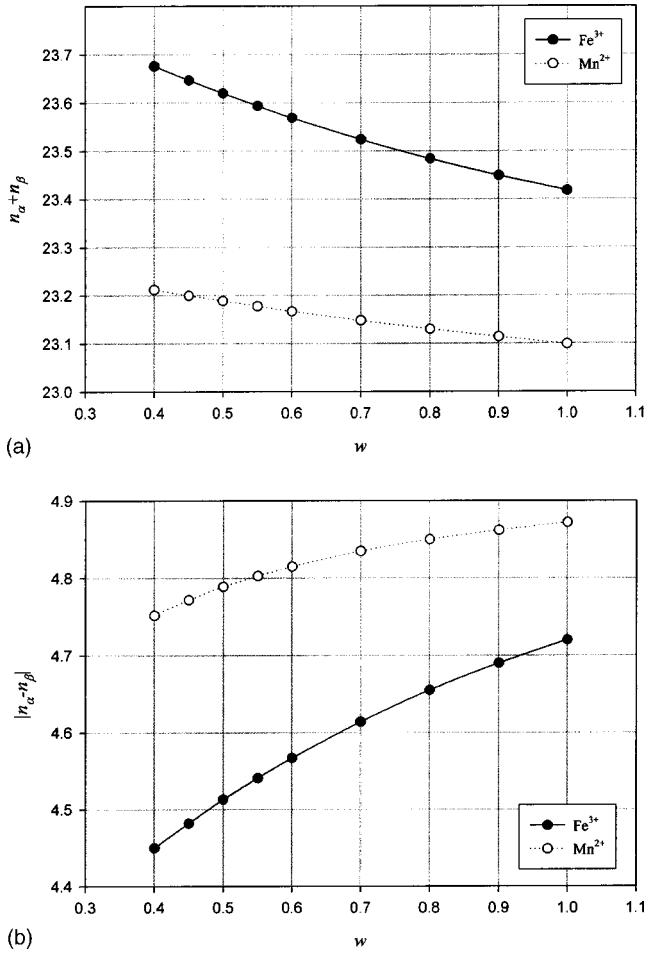

FIG. 3. Depolarized Mulliken population $(n_\alpha + n_\beta)$ and the absolute value of the polarized Mulliken population $|n_\alpha - n_\beta|$ of Fe^{3+} and Mn^{2+}.

theory, both polarized and depolarized Mulliken populations of d orbits of magnetic ions split to e_g and t_{2g} orbits. If we plot the polarization rate (the ratio of the polarized Mulliken population to the depolarized one) of d orbits of Mn^{2+} and Fe^{3+} versus w (Fig. 4), we find that in Fe^{3+} t_{2g} orbits are less polarized than e_g and that in Mn^{2+} e_g orbits are less polarized than the t_{2g} submanifold, which represents the different local symmetries of Mn^{2+} and Fe^{3+}. In the normal spinel structure, Fe^{3+} and Mn^{2+} ions are located at octahedral and tetrahedral sites, respectively. At an octahedral site, the e_g orbits ($d_{3z^2-r^2}$ and $d_{x^2-y^2}$) extend directly toward the O^{2-} at the vertexes and the t_{2g} orbits (d_{xy}, d_{yz}, and d_{zx}) extend toward the edges. Thus, the e_g orbits hybridize more heavily with the orbits of O^{2-} than t_{2g} orbits and, as a result, the e_g orbits are less polarized than t_{2g} orbits. On the other hand, at a tetrahedral site, the e_g orbits extend toward the edge and the t_{2g} orbits toward the O^{2-} (not directly). Thus, the hybridization between the t_{2g} orbits and orbits of O^{2-} is stronger than that between the e_g orbits and the orbits of O^{2-}. As a result, the t_{2g} orbits are less polarized than the e_g orbits. If we compare a $4d$ orbit and its $3d$ counterpart, we find that a $4d$ orbit is always less polarized than its $3d$ coun-

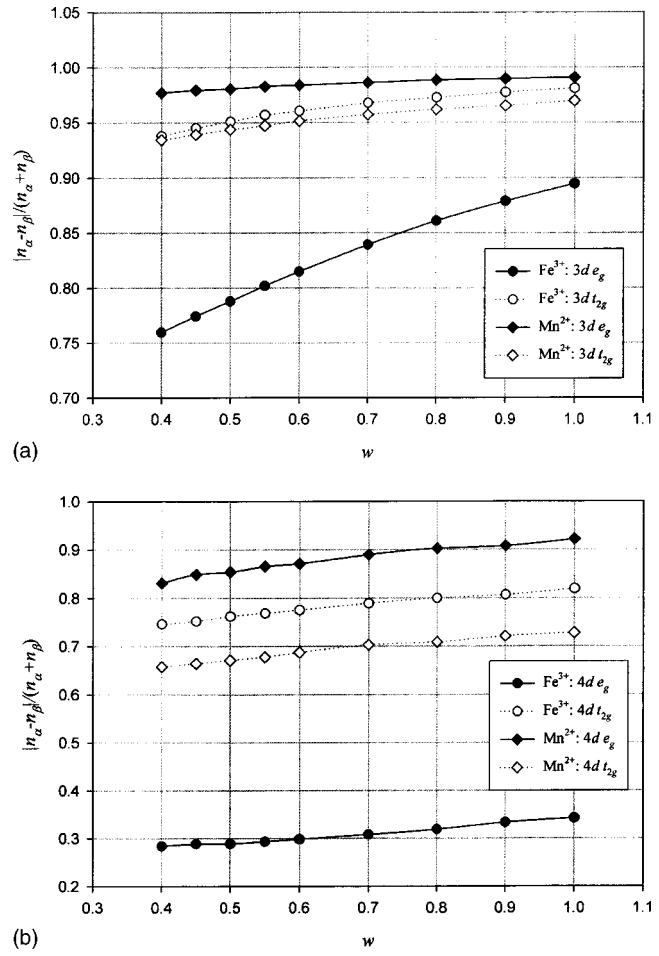

FIG. 4. Polarization ratio $|n_\alpha - n_\beta|/(n_\alpha + n_\beta)$ of Fe^{3+} and Mn^{2+}.

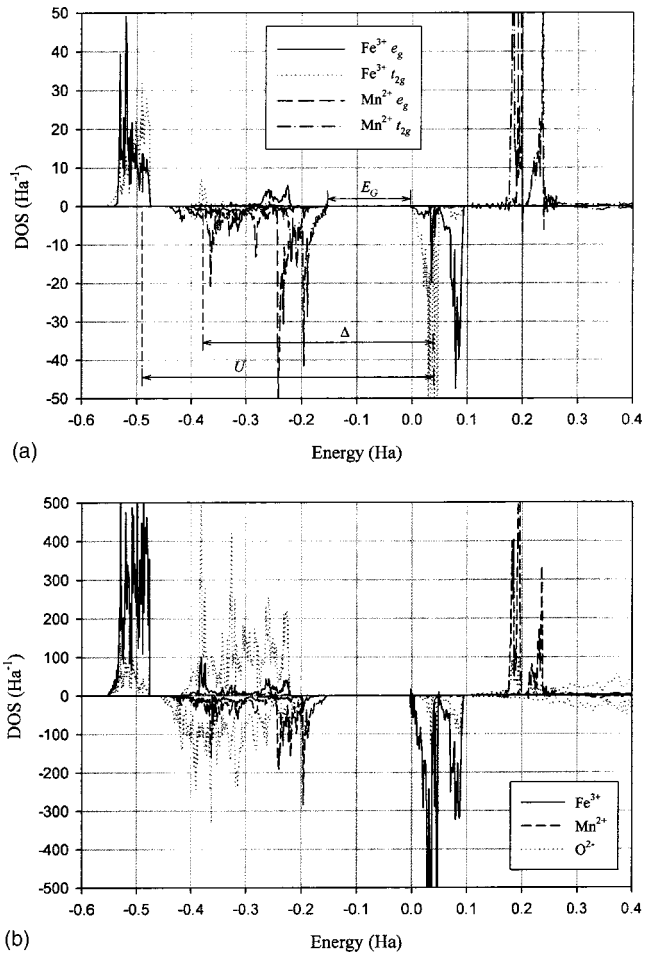

FIG. 5. The DOS of $MnFe_2O_4$ projected on sites and orbits.

terpart. This is the result of the fact that the $4d$ orbit is always more extensive than its $3d$ counterpart and consequently hybridized more heavily with the orbits of O^{2-}.

If we compare a d orbit of Mn^{2+} and its counterpart of Fe^{3+}, we find that a d orbit of Mn^{2+} is always more polarized that its counterpart of Fe^{3+}. One reason is that although a d orbit of Mn^{2+} is more extensive than its counterpart of Fe^{3+} and the length of the Mn-O bond ($\sim$1.98 Å) is little shorter than that of the Fe-O bond ($\sim$2.01 Å), the difference of the p-d transfer integral (t_{pd}) between the e_g and t_{2g} orbits for Mn^{2+} should be weaker than that for Fe^{3+} due to the tetrahedral local symmetry of Mn^{2+}, in which there is no orbit of Mn^{2+} extending directly toward the O^{2-} ion. The other reason is that since the configuration $|d^6L\rangle$ for the $[MnO_4]^{6-}$ complex has a higher energy (more unstable) than that for the $[FeO_6]^{9-}$ complex, Mn^{2+} has a higher Δ than Fe^{3+}. If we focus on the dependence of polarization rate on w, we find that when w decreases the polarization rates of all the d orbits of magnetic ions decrease. The Fork term underestimates the hybridization. On the other hand, the LSDA term in the Becke exchange overestimates the electron-electron correlation and consequently overestimates the hybridization. Since w is the linear interpolation coefficient to balance the Fock and the Becke exchanges, we can expect that, when w decreases, the covalent effect between the magnetic ions and O^{2-} will increase and as a result the polarization rates of the d orbits will decrease. However, different d orbits exhibit different sensitivity to w. In Fig. 4, we find that $3d\ e_g$ is more sensitive than $3d\ t_{2g}$ in Fe^{3+}, and that $3d\ t_{2g}$ is more sensitive than $3d\ e_g$ in Mn^{2+}. This is more evidence that $3d\ e_g$ is more heavily hybridized with the orbits of O^{2-} than $3d\ t_{2g}$ in Fe^{3+}, and that $3d\ t_{2g}$ is more heavily hybridized with the orbits of O^{2-} than $3d\ e_g$ in Mn^{2+} due to the local symmetry of the A (tetrahedral) and B (octahedral) sites.

Also, we have considered the density of states (DOS) projected on sites and the d orbits of magnetic ions for the FI-1 magnetic structure at $w = 40\%$ calculated using an optimized basis set (Fig. 5). Compared to the DOS given by LSDA (Ref. 72) or GGA,[73] the DOS given by our calculation is quite different. First, the DOS given by LSDA or GGA implied that $MnFe_2O_4$ is half metallic, where the spin-down Mn^{2+} and the spin-down Fe^{3+} d bands overlapped each other and crossed over the Fermi level. However, in our calculation, the DOS shows that $MnFe_2O_4$ is a typical insulator with a band gap between the spin-down Mn^{2+} and spin-down Fe^{3+} d bands. Second, the DOS given by LSDA or GGA implied that $MnFe_2O_4$ is a typical Mott insulator for both Fe^{3+} and Mn^{2+}, in which the ligand p band is located

at a lower energy than the *d* bands of transition-metal ions in the valence band. However, in our calculation, the Fe^{3+} and O^{2-} system is a typical charge-transfer insulator and the Mn^{2+} and O^{2-} system is an interim state between the Mott insulator and charge-transfer insulator. The DOS projected on the O^{2-} site shows that there is a wide (compared to the *d* bands of magnetic ions) O^{2-} band extending from -0.42 to -0.22 hartree (the top of the valence band) for spin-up electrons and from -0.45 to -0.16 hartree (the top of the valence band) for spin-down electrons. If we plot the DOS projected on Fe^{3+} and O^{2-} sites together, we find that in the region around the Fermi level (-0.6 to 0.4 hartree) a *d* band (e_g or t_{2g}) of Fe^{3+} splits into three sub-bands, which separate from each other. In these sub-bands, two of them are characteristic of a narrow bandwidth (about 0.05 hartree) but have opposite spin directions, which correspond to the localized spin-up and -down *d* states of Fe^{3+}. It should be noted that the spin-up localized *d* band of Fe^{3+} is located at a lower energy than the O^{2-} band at the top of the valence band, which is characteristic of a typical charge-transfer insulator, such as NiO.[17,18] Also, one of the sub-bands overlaps with the O^{2-} band at the top of the valence band as a result of the hybridization between the *d* orbits of Fe^{3+} and the orbits of O^{2-}. However, if we plot the DOS projected on Mn^{2+} and O^{2-} sites together, the spin-down localized (narrow) sub-band is located at the top of valence band and overlaps with the O^{2-} band, which is an interim state between the Mott insulator and the charge-transfer insulator.

In fact, the above differences between the DOS given by LSDA or GGA and that given by our calculation may be simplified to three important parameters of transition-metal oxides E_G, U, and Δ. In Fig. 5(a), we show schematically U and Δ for Fe^{3+}. It is clear that we have extracted a U value from the t_{2g} bands. There also exists a U value associated with e_g bands. The same applies for the extraction of Δ from Fig. 5(a). There also corresponds a set of U and Δ values for the Mn^{2+} ion. E_G is simply the separation between the valence and conduction bands at the Fermi level. First, we consider E_G and U, which are closely related in $MnFe_2O_4$. Intuitively, an overestimated electron-electron correlation in LSDA or GGA implies easier transfer of $3d$ electrons from one magnetic ion to another, which means a higher conductivity at finite temperature or a narrower band gap, which also means a lower potential barrier or a smaller U. In the DOS given by LSDA or GGA, if U's of Fe^{3+} and Mn^{2+} were increased, the spin-down Mn^{2+} and spin-down Fe^{3+} *d* bands would be separated and, consequently, an insulating result would be yielded. Unfortunately, since LSDA or GGA overestimates the electron-electron correlation, U in LSDA or GGA was insufficient to separate the spin-down Mn^{2+} and spin-down Fe^{3+} *d* bands and consequently to open a band gap. On the other hand, the underestimated electron-electron correlation yields the opposite result as predicted by LSDA or GGA. In HF calculations, U is much larger than the experimental value, and thus, E_G is much larger than the experimental value. Since the functional chosen in our calculation is a mixture of Fock and Becke exchanges with a variable weight w, it is possible to study the dependence of

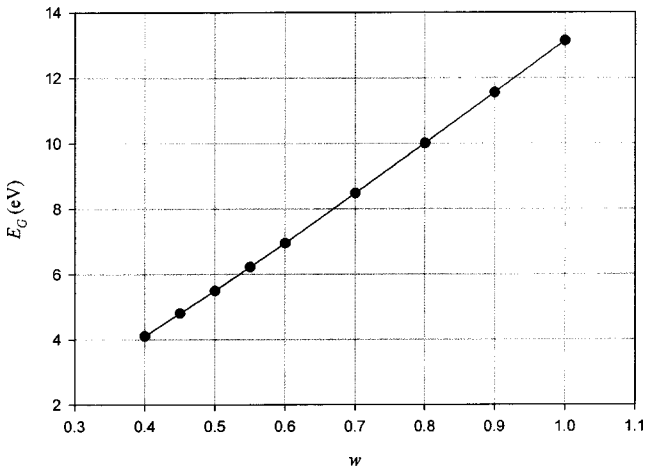

FIG. 6. E_G extracted from the DOS.

E_G and U on w (Figs. 6 and 7), which reveals the opposite natures of HF and LSDA (or GGA) in approximating the electron-electron correlation. In the configuration interaction (CI) calculation, U is the energy difference between two configurations d^6 and d^4, corresponding to an extra localized *d* electron and *d* hole, respectively, if we neglect the direct exchange (J) that is usually in order of 10^{-2} eV for transition-metal oxides. Thus, if we interpret the valence bands as the states of a probing hole and the conduction bands as the states of a probing electron, U could be directly mapped to the energy difference between the localized *d* bands in the valence and conduction bands. Further, to remove the band effect introduced by translational symmetry of the crystal, we calculated the average of a localized *d* band using its DOS as the weight. As shown in Fig. 7, U decreases when w decreases. For example, at $w=40\%$, U of the Mn^{2+} e_g band is about 0.46 hartree$\approx$11.7 eV and that of the Mn^{2+} t_{2g} band is about 0.41 hartree$\approx$11.2 eV. At $w=100\%$, U of the Mn^{2+} e_g band is about 0.82 hartree$\approx$22.3 eV and that of the Mn^{2+} t_{2g} band is about 0.80 hartree$\approx$21.8 eV. It should be noted that, under Hartree-Fock approximation, U should be equal to U_b. In fact, Towler *et al.* evaluated U for MnO at the experimental lattice parameter using the radial part of a *d*

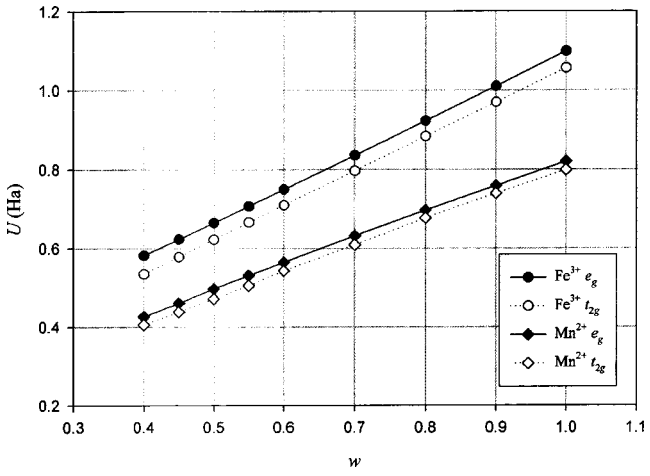

FIG. 7. U of Fe^{3+} and Mn^{2+} extracted from the DOS.

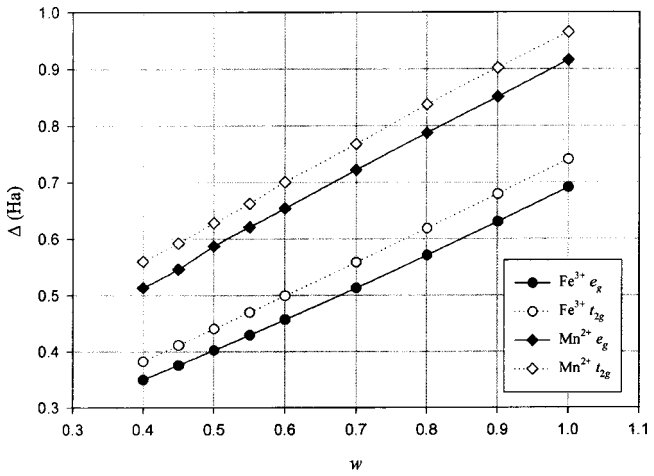

FIG. 8. Δ of Fe^{3+} and Mn^{2+} extracted from the DOS.

wave function of Mn^{2+} optimized for bulk MnO by pure Hartree-Fock calculation, and obtained $U=0.861$ hartree ≈ 23 eV.[30] When w decreases, more and more electron-electron correlation is taken into account and as a result U decreases. Since the basis sets used in our calculation are optimized for pure Hartree-Fock calculations, the calculations will diverge when w is smaller than 40% for the FI-1 magnetic structure.

Second, we consider U and Δ, which classify the insulating transition-metal oxides. Analogous to U, Δ is extracted from the DOS as the energy difference between the localized d bands in conduction bands and the d bands submerged into the O^{2-} bands, and is plotted in Fig. 8. Since both Mn^{2+} and Fe^{3+} are magnetic in $MnFe_2O_4$, we have a complex insulator. Using the values of U and Δ deduced from the Mn^{2+} bands, we may classify $MnFe_2O_4$ as an interim insulator since $U \approx \Delta$. However, using the values of U and Δ deduced from the Fe^{3+} bands, we may classify $MnFe_2O_4$ as a charge-transfer insulator since $U > \Delta$. The CI analyses of photoemission data suggest that MnO is an interim between the Mott insulator and charge-transfer insulator[74–76] and that hematite (α-Fe_2O_3) is a typical charge-transfer insulator,[77,78] which indirectly supports the above result. However, if we focus on the band gap, which is between the spin-down full d band of Mn^{2+} and the spin-down empty d band of Fe^{3+}, the substantial contribution to the conduction of intrinsic $MnFe_2O_4$ is the process

$$Mn^{+} + Fe^{3+} \leftrightarrow Mn^{3+} + Fe^{2+}, \tag{6}$$

which is a spin-conservative transfer of electrons between Mn^{2+} and Fe^{3+}. Also, both U and Δ monotonously decrease when w decreases (Figs. 7 and 8), which is qualitatively compatible with the fact that the absolute value of J_{AB} increases monotonously as w decreases.

TABLE I. Comparison between theory and experiment.

	J_{AB} (K)		J_{BB} (K)	
	Normal	Inverse	Normal	Inverse
This calculation	−15.3[a]	−14.5[b]	11.3[a]	7.3[b]
	−18.3[c]	−21.4[d]	−4.4[c]	−12.0[d]
Experiment	−22.7,[e]	−19.1[f]	−3.0[f]	
HF	−4.7	−4.4	10.2	6.6
LSDA				
GGA	−464[g]			

[a]Using optimized basis sets and evaluated at $w=40\%$.
[b]Using optimized basis sets and evaluated at $w=50\%$.
[c]Using the basis sets with expanded $3d$ wave functions and evaluated at $w=30\%$.
[d]Using the basis sets with expanded $3d$ wave functions and evaluated at $w=40\%$
[e]Reference 66.
[f]Reference 68.
[g]Reference 73.

IV. CONCLUSION

In Table I, we summarize and compare the values of J_{AB} and J_{BB} calculated by us with the experimental values. The calculated J_{AB} and J_{BB} are closer to the experimental values than either HF or GGA for $MnFe_2O_4$, by using the basis sets with expanded $3d$ wave functions of Fe^{3+} ions at $w=30\%$. The calculated DOS shows that $MnFe_2O_4$ is an insulator, which is qualitatively in agreement with experiments. Also the calculated DOS shows that the Fe^{3+} and O^{2+} system is a typical charge-transfer insulator and that the Mn^{2+} and O^{2-} system is an interim between a Mott insulator and charge-transfer insulator, both of which are indirectly supported by experiments. The dependencies of U and Δ on w are extracted from the calculations, and show qualitative compatibility with the dependence of J_{AB} on w. In conclusion our calculated results yield a set of magnetic and electronic properties, which are consistent with experimental observations. The fact that the calculations are able to be generally applicable to various experiments lends some credibility to our calculation.

ACKNOWLEDGMENTS

We wish to thank Dr. Kristl Hathaway for suggestions in the formulation of these calculations. Also, we wish to thank Dr. Bernardo Barbiellini for helpful discussions and Professor Allan Widom for critical discussions. This work has benefited from the allocation of computer time at Northeastern University Scientific Computational Center. This research was supported by ONR.

[1] E. W. Gorter, Philips Res. Rep. **9**, 295 (1954).
[2] J. M. Hastings and L. M. Corliss, Phys. Rev. **104**, 328 (1956).
[3] J. Smith and J. Wijn, *Ferrites* (Wiley, New York, 1959).
[4] W. H. von Aulock, *Handbook of Microwave Ferrite Materials* (Academic, New York, 1965).
[5] P. W. Anderson, Phys. Rev. **115**, 2 (1959).
[6] J. Hubbard, Proc. R. Soc. London, Ser. A **276**, 238 (1963).
[7] J. Kanamori, Prog. Theor. Phys. **30**, 275 (1963).

[8] H. A. Kramers, Physica (Amsterdam) **1**, 1934 (1934).
[9] P. W. Anderson, in *Magnetism*, edited by G. T. Rado and H. Suhl (Academic, New York, 1963), Vol. I, p. 25.
[10] P. W. Anderson, in *Solid State Physics*, edited by H. Ehrereich, F. Seitz, and D. Turnbull (Academic, New York, 1963), Vol. 14, p. 99.
[11] N. F. Mott, Proc. Phys. Soc. London **49**, 72 (1937).
[12] N. F. Mott, Proc. Phys. Soc., London, Sect. A **62**, 416 (1949).
[13] N. F. Mott, Can. J. Phys. **34**, 1356 (1956).
[14] N. F. Mott, Philos. Mag. **6**, 287 (1961).
[15] N. F. Mott, *Metal-Insulator Transitions* (Taylor & Francis, London, 1990).
[16] F. K. Lotgering, J. Phys. Chem. Solids **25**, 95 (1964).
[17] A. Fujimori and F. Minami, Phys. Rev. B **30**, 957 (1984).
[18] G. A. Sawatzky and J. Allen, Phys. Rev. Lett. **53**, 2339 (1984).
[19] J. Zaanen, G. A. Sawatzky, and J. W. Allen, Phys. Rev. Lett. **55**, 418 (1985).
[20] J. Zaanen and G. A. Sawatzky, Can. J. Phys. **65**, 1262 (1987).
[21] J. Zaanen and G. A. Sawatzky, J. Solid State Chem. **88**, 8 (1990).
[22] R. G. Shulman and S. Sugano, Phys. Rev. **130**, 506 (1963).
[23] R. E. Watson and A. J. Freeman, Phys. Rev. A **134**, A1526 (1964).
[24] J. Hubbard, D. E. Rimmer, and F. R. A. Hopgood, Proc. Phys. Soc. London Sect. A **88**, 13 (1966).
[25] D. E. Ellis, A. J. Freeman, and P. Ros, Phys. Rev. **176**, 688 (1968).
[26] D. R. Hartree, Rep. Prog. Phys. **11**, 113 (1948).
[27] C. C. J. Roothaan, Rev. Mod. Phys. **23**, 69 (1951).
[28] J. A. Pople and R. K. Nesbet, J. Chem. Phys. **22**, 571 (1954).
[29] C. C. J. Roothaan, Rev. Mod. Phys. **32**, 179 (1960).
[30] M. D. Towler, N. L. Allan, N. M. Harrison, V. R. Saunders, W. C. Mackrodt, and E. Aprà, Phys. Rev. B **50**, 5041 (1994).
[31] M. T. Hutchings and E. J. Samuelsen, Phys. Rev. B **6**, 3447 (1972).
[32] R. J. Powell and W. E. Spicer, Phys. Rev. B **2**, 2182 (1970).
[33] S. Hüfner, J. Osterwald, T. Riesterer, and F. Hulliger, Solid State Commun. **52**, 793 (1984).
[34] P. Hohenberg and W. Kohn, Phys. Rev. **136**, B864 (1964).
[35] W. Kohn and L. J. Sham, Phys. Rev. **140**, A1133 (1965).
[36] U. von Barth and L. Hedin, J. Phys. C **5**, 1629 (1972).
[37] A. K. Rajagopal and J. Callaway, Phys. Rev. B **7**, 1912 (1972).
[38] O. K. Anderson, H. L. Skriver, H. Nohl, and B. Johansson, Pure Appl. Chem. **52**, 93 (1979).
[39] K. Terakura, A. R. Williams, T. Oguchi, and J. Kübler, Phys. Rev. Lett. **52**, 1830 (1984).
[40] K. Terakura, A. R. Williams, T. Oguchi, and J. Kübler, Phys. Rev. B **30**, 4734 (1984).
[41] A. Zunger, J. P. Perdew, and G. L. Oliver, Solid State Commun. **34**, 933 (1980).
[42] J. P. Perdew and A. Zunger, Phys. Rev. B **23**, 5048 (1981).
[43] J. P. Perdew and Y. Wang, Phys. Rev. B **33**, 8800 (1986).
[44] J. P. Perdew and Y. Wang, Phys. Rev. B **45**, 13 244 (1992).
[45] J. P. Perdew, J. A. Chevary, S. H. Vosko, K. A. Jackson, M. R. Pederson, D. J. Singh, and C. Fiolhais, Phys. Rev. B **46**, 6671 (1992).
[46] J. P. Perdew, K. Burke, and M. Ernzerhof, Phys. Rev. Lett. **77**, 3865 (1996).
[47] A. D. Becke, Phys. Rev. A **38**, 3098 (1988).
[48] A. D. Becke, J. Chem. Phys. **96**, 2155 (1992).
[49] V. I. Anisimov, J. Zaanen, and O. K. Anderson, Phys. Rev. B **44**, 943 (1991).
[50] P. Wei and Z. Q. Qi, Phys. Rev. B **49**, 10 864 (1994).
[51] J. Hugel and M. Kamal, Solid State Commun. **100**, 457 (1996).
[52] J. Hugel and M. Kamal, J. Phys.: Condens. Matter **9**, 647 (1997).
[53] A. Svane and O. Gunnarsson, Phys. Rev. Lett. **65**, 1148 (1990).
[54] Z. Szotek, W. M. Temmerman, and H. Winter, Phys. Rev. B **47**, 4029 (1993).
[55] P. Dufek, P. Blaha, V. Sliwko, and K. Schwarz, Phys. Rev. B **49**, 10 170 (1994).
[56] F. J. Morin, Bell Syst. Tech. J. **37**, 1047 (1958).
[57] K. Knox, R. G. Shulman, and S. Sugano, Phys. Rev. **130**, 512 (1963).
[58] R. Dovesi, C. Roetti, C. Freyria-Fava, E. Aprà, V. R. Saunders, and N. M. Harrison, Philos. Trans. R. Soc. London, Ser. A **341**, 203 (1992).
[59] A. D. Becke, Phys. Rev. A **33**, 2786 (1986).
[60] A. D. Becke, ACS Symp. Ser. **394**, 165 (1989).
[61] A. D. Becke, J. Chem. Phys. **98**, 1372 (1993).
[62] A. D. Becke, J. Chem. Phys. **98**, 5648 (1993).
[63] M. Catti, G. Valerio, and R. Dovesi, Phys. Rev. B **51**, 7441 (1995).
[64] V. R. Saunders, R. Dovesi, C. Roetti, M. Causà, N. M. Harrison, R. Orlando, and C. M. Zicovich, computer code CRYSTAL98, User's manual (Theoretical Chemistry Group, University of Turin, Torino, Italy, 1999).
[65] R. W. G. Wyckoff, *Crystal Structures*, 2nd ed. (Wiley, New York, 1967), Vol. 3, p. 75.
[66] A. J. Heeger and T. W. Houston, Phys. Rev. **133**, A661 (1964).
[67] V. C. Rakhecha, L. M. Rao, N. S. S. Murthy, and B. S. Srinivasan, Phys. Lett. **40A**, 101 (1972).
[68] W. Wegener, D. Scheerlinck, E. Legrand, and S. Hautecler, Solid State Commun. **15**, 345 (1974).
[69] X. Zuo, and C. Vittoria (unpublished).
[70] M. Bonfante, B. Hennion, F. Moussa, and G. Pepy, Solid State Commun. **10**, 553 (1972).
[71] M. Kohgi, Y. Ishikawa, and Y. Endoh, Solid State Commun. **11**, 391 (1972).
[72] M. Pénicaud, B. Siberchicot, C. B. Sommers, and J. Kübler, J. Magn. Magn. Mater. **103**, 212 (1992).
[73] D. J. Singh, M. Gupta, and R. Gupta, Phys. Rev. B **65**, 064432 (2002).
[74] A. Fujimori, N. Kimizuka, T. Akahane, T. Chiba, S. Kimura, F. Minami, K. Siratori, M. Taniguichi, S. Ogawa, and S. Suga, Phys. Rev. B **42**, 7580 (1990).
[75] J. van Elp, R. H. Potze, H. Eskes, R. Berger, and G. A. Sawatzky, Phys. Rev. B **44**, 1530 (1991).
[76] R. J. Lad and V. E. Henrich, Phys. Rev. B **38**, 10 860 (1988).
[77] A. Fujimori, M. Saeki, N. Kimizuka, M. Taniguchi, and S. Suga, Phys. Rev. B **34**, 7318 (1986).
[78] R. J. Lad and V. E. Henrich, Phys. Rev. B **39**, 13 478 (1989).